

Ageing and collapse in gels with long-range attractions†

Lisa J. Teece,^a Malcolm A. Faers^b and Paul Bartlett^{*a}

Received 3rd July 2010, Accepted 21st October 2010

DOI: 10.1039/c0sm00626b

We report measurements on the ageing dynamics of a colloid–polymer mixture with a large polymer–colloid size ratio of 0.62. Quenched into a two-phase region the system gels and forms a network with a characteristic radius R_c . We find three distinct regimes in the time evolution of $R_c(t)$, reminiscent of the linear, late and gravity-dominated regimes of coarsening seen in classical spinodal decomposition kinetics of binary fluids. In the early stages of gelation, we observe a peak in the time-dependent structure factor $S(q, t)$ which is stationary in q and grows in intensity characteristic of a linear-Cahn regime. The domain size then coarsens continuously with the age t of the sample. In the late stages the domain size follows the approximate algebraic law, $R_c \sim t^\theta$. The growth exponent θ is a strong function of the quench depth: for small polymer concentrations θ is significantly larger than for large polymer concentrations. The gel networks formed are transient, and in the final stages of phase separation, collapse under gravity when the correlation length of the gel becomes $\sim 2\pi$ times the capillary length.

1. Introduction

Systems far from equilibrium often display startlingly complex dynamics even while their equilibrium behaviour may be quite mundane. A particular striking example is a colloidal suspension of spheres of packing fraction ϕ with weak attractive interactions (of strength U_0). Equilibrium leads to phase separation but if rapidly concentrated this system ‘gels’ and forms a low-density disordered soft solid.¹ Gels are fascinatingly complex materials because they are highly nonlinear, transient and nonequilibrium in nature. They contain a space spanning network of particle chains which is able to support a stress, yet form at surprisingly low packing fractions (down to fractions of a percent by volume) and have no obvious counterparts in atomic or molecular systems. Understanding and controlling gelation is central to a number of technological areas, ranging from the traditional food,² personal products and pesticide industries to protein crystallography³ and various diseases of protein aggregation such as cataracts,⁴ sickle cell anaemia,⁵ Alzheimer’s disease and amyloid fibril growth. In addition intelligent design of particle gels is critical for several emerging materials applications, such as the preparation of sol–gel printing inks used to print 3D-nanostructures such as micro-fuel cells, photonic crystals and gas sensors. Yet despite the technological and scientific importance of gelation the molecular processes involved in their formation remain uncertain and hotly debated.

Particular attention has focussed recently on systems with isotropic short-range attractions, where the range of the potential Δ/a in units of the particle radius a is less than 10%. By combining experiment, simulation and theory the mechanism of gelation in systems with $\phi \leq 0.4$ has now been relatively firmly established.^{6–11} Fig. 1 (a) summarizes the currently accepted state diagram. The attractive glass transition intersects the gas–liquid

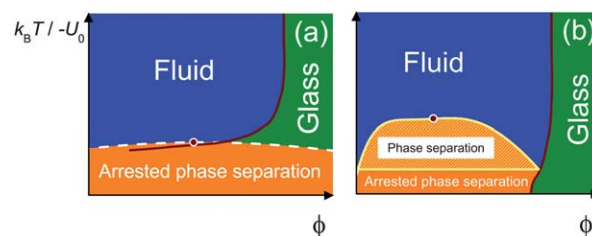


Fig. 1 Schematic diagram which illustrates the effect of changing the range Δ of the attractive interactions upon the relative positions of the liquid–gas coexistence line and the glass line in a system of hard-spheres of radius a with a square-well attraction of width Δ/a and depth U_0 . In (a), where the attraction is short-ranged, the glass line intersects the binodal just below the critical temperature while (b) illustrates the case for a long-range attraction.

binodal just to the right of the critical point (circled). A colloidal suspension quenched into the two-phase gas–liquid region undergoes an initial spinodal decomposition (SD) into colloid-rich and colloid-poor regions. However the phase separation kinetics are almost immediately arrested as the concentration of the high density regions inside the gel cross the attractive glass line and the structure is frozen. In contrast, much less is known about gelation with long-range attractions even though this situation is important in many realms of nanoscience. Theoretical work¹² suggests that increasing the range Δ/a of the attraction has a number of effects on the phase behaviour, which are sketched schematically in Fig. 1 (b): first, the region of gas–liquid separation, which is metastable at small Δ/a , should increase in stability relative to the glass-line, and second the gas–liquid boundary should become more sharply curved. Thus at large Δ/a one imagines there should be a range of compositions (hashed in Fig. 1 (b)) at which spinodal decomposition will progress to full phase separation, without being arrested – presumably without gelation. Still deeper quenches could generate kinetic arrest and gel formation.

In this paper we explore experimentally what happens when a colloid–polymer mixture with a long range attraction

^aSchool of Chemistry, University of Bristol, Bristol, BS8 1TS, UK. E-mail: p.bartlett@bristol.ac.uk

^bBayer CropScience AG, 40789 Monheim am Rhein, Germany

† This paper is part of a *Soft Matter* themed issue dedicated to the International Soft Matter Conference 2010.

(polymer–colloid size ratio ~ 0.62) is quenched deep into a two-phase region, under the influence of gravity. For all polymer concentrations studied here we find that, in contrast to short-range attractive systems, the kinetics of phase separation are not arrested on any accessible experimental time scales. Instead a transient network is formed by a phase separation process analogous to spinodal decomposition which continuously coarsens. We use a combination of rheology and laser-scanning confocal microscopy to follow quantitatively the competition between the thermal coarsening of this network, as it evolves very slowly towards equilibrium, and the gravitational stresses which act on the gel. We find that the characteristic length scale of the network, R_c , grows continuously with the age t of the sample until R_c reaches a critical value at which point the gel collapses in the gravitational field.

2. Materials and methods

2.1. Colloidal dispersion

We use a dispersion composed of a low polydispersity emulsion of poly(dimethyl siloxane) (Dow Corning, PDMS DC200 10cSt) dispersed in a refractive index-matched mixed solvent of 1,2-ethane diol (EG) and water. The emulsion was stabilized against aggregation by a combination of commercial non-ionic surfactants (PEO-PPO-PEO, M_w 4950, 30% PEO, Pluronic P103, BASF and tristyrilphenol ethoxylate, 16EO, Tanatex) and the anionic surfactant sodium bis(2-ethyl 1-hexyl) sulfosuccinate (Fluka, Na-AOT). The addition of Na-AOT increased the stability of the system by generating a slight negative charge on the emulsion drops. The emulsion sample had a hydrodynamic radius of $a = 316 \pm 11$ nm and a size polydispersity of 0.17 ± 0.07 , as measured with dynamic light scattering (DLS). Particular care was taken to closely match the refractive index of the emulsion to the continuous phase by meticulously adjusting the proportion of EG in the solvent mixture to minimize the intensity of light scattered at $\lambda = 543$ nm. Almost completely transparent samples were obtained at a mass fraction of EG of $w_{EG} = 0.59$. The index-matched continuous phase had a viscosity of 5.42 mPa s ± 0.02 mPa s, as measured by capillary viscometry, a refractive index of 1.396 at 543 nm, and a density of $\rho_m = 1.067$ g cm $^{-3}$ ± 0.005 g cm $^{-3}$. The density of the PDMS oil is lower than the continuous phase ($\rho_c = 0.934$ g cm $^{-3}$ ± 0.006 g cm $^{-3}$) so that the dispersions cream in a gravitational field. The density mismatch of the oil is $\Delta\rho = \rho_c - \rho_m = -0.13 \pm 0.01$ g cm $^{-3}$. To screen out any long-range electrostatic interactions and generate hard-sphere-like interactions between the emulsion drops we add 3 mM potassium chloride to all of our samples.

2.2. Polymer characterization

To induce an attractive interaction in our system we add the anionic polyelectrolyte xanthan (Kelco, $M_w = 4.66 \times 10^6$ g mol $^{-1}$). Xanthan is a widely-studied ionic biopolymer which consists of a main chain of β -1,4 linked D-glucose units with a side chain, of three sugar units and two carboxylate anions, attached to every other main-chain residue.¹³ The negative charges on both the polymer and colloid and the presence of a steric layer ensures that the polymer is not adsorbed on to the surface of the emulsion drops. A xanthan stock with concentration $c_p/c_p^* = 12$ was

prepared by mixing the required mass of xanthan powder (used as supplied) with an index-matched mixture of EG and water. The solution was gently stirred with a magnetic stirrer for 72 h until a homogeneous appearance was achieved. When preparing individual samples, the xanthan stock was diluted with appropriate amounts of EG and water and then gently stirred magnetically for 3 h.

We use viscometry and dynamic light scattering to determine the conformation of xanthan in the mixed EG/water solvent. At room temperature xanthan dissolves in aqueous solutions as a double-stranded helical structure with a high degree of stiffness. Low molecular weight fractions are almost totally stiff but light scattering,¹³ viscometry^{14,15} and sedimentation studies suggests that above a relative molecular weight of $M \sim 3 \times 10^5$ g mol $^{-1}$ it behaves as a classical semi-flexible polymer characterized by three parameters: the mass per unit contour length, M_L ; the Kuhn statistical segment length, λ^{-1} ; and the hydrodynamic diameter of the chain, d . Sho *et al.* reported values of $\lambda^{-1} = 212$ nm, a diameter of $d = 2.2$ nm, and a mass per unit contour length of $M_L = 1940$ daltons nm $^{-1}$, from an analysis of intrinsic viscosity data in water.¹⁵ For our xanthan sample we measured an intrinsic viscosity in water of 5090 cm 3 g $^{-1}$ and 2320 cm 3 g $^{-1}$ in the index-matched EG/water mixture ($w_{EG} = 0.59$). The lower value in the mixed solvent suggests that the strength of the hydrogen-bonds, which bind together the double-helical structure of xanthan and which result in the large Kuhn length in water, are weaker in the mixed solvent. This observation is consistent with the trend¹⁶ that the extent of hydrogen bonding association is lower in alcohol-water mixtures than in pure H $_2$ O. The mass per unit contour length and the chain diameter of xanthan are a function of the chemical structure of the backbone of the polymer and so remain unaltered as water is replaced by EG. Assuming $M_L = 1940$ nm $^{-1}$, and $d = 2.2$ nm we estimate a Kuhn length of *ca.* 78 nm at $w_{EG} = 0.59$, using the Bohdanecky¹⁷ implementation of the Yamakawa and Fujii model¹⁸ to calculate the intrinsic viscosity of a worm-like chain. The Kuhn length is considerably smaller than the value generally accepted for water ($\lambda^{-1} = 240$ – 255 nm),^{13–15} reflecting the increased flexibility of the polymer in the mixed solvent. An expression for the radius of gyration of a monodisperse worm-like chain has been derived by Benoit and Doty,¹⁹ while the effect of chain polydispersity has been quantified by Schmidt.²⁰ Assuming a Schultz distribution, with a width chosen to match the measured chain dispersity ($M_w/M_n = 1.35$), the z -average mean radius of gyration is $r_g = 194$ nm. The overlap concentration $c_p^* = 3M_w/(N_A 4\pi r_g^3)$ is about 0.25 g dm $^{-3}$.

2.3. Colloid–polymer mixtures

Samples were prepared by mixing together colloid- and polymer-stock dispersions with a solution of the fluorescent dye rhodamine-B (Aldrich), before finally diluting with a mixture of EG and water. The proportions of each stock were adjusted to give samples with a fixed EG mass fraction of $w_{EG} = 0.59$, a salt concentration of 3×10^{-3} mol dm $^{-3}$, and a rhodamine-B concentration of 0.02 g dm $^{-3}$ in the continuous phase. The colloid–polymer mixtures were carefully homogenized to minimize the number of air bubbles entrained within the sample which can destroy the delicate bicontinuous network when they

escape. Directly after homogenization phase separation starts so the sample age was estimated from the end of homogenization. The sample was then rapidly transferred to the specially-fabricated cells described in Sec. 2.4.

Each emulsion drop is surrounded by a spherical shell of solvent which is depleted of polymer molecules as a consequence of the loss of configurational entropy a polymer suffers near a surface. When the layers around two particles overlap the volume of the polymer depleted region is reduced and a net attraction is generated. The strength of this attraction is a function of the polymer concentration while its range is controlled by the relative size of polymer and particle. We use a large polymer combined with a relatively small particle to ensure that the range of the attractive depletion forces, parameterized by the size ratio $q_R = r_g/a \approx 0.62 \pm 0.04$, is large. The strength of the isotropic attractions was “tuned” by adjusting the polymer concentration in the reservoir, c_p . We calculate c_p from the total polymer concentration c_p^{tot} added to the sample using the expression $c_p^{\text{tot}} = \alpha c_p$, where α is the fraction of available free volume. For the free volume fraction α we use the standard scaled-particle result,²¹

$$\alpha = (1 - \phi) \exp(-Af - Bf^2 - Cf^3) \quad (1)$$

where $f = \phi/(1 - \phi)$ and the coefficients are $A = (1 + q_s)^3 - 1$, $B = 3q_s^3(q_s + 3/2)$, and $C = 3q_s^3$. Here $q_s = \delta/a$ is the relative thickness (δ) of the depletion zone around a sphere of radius a . The width of the depletion region shrinks with increasing polymer concentration, from a value of order q_R in dilute solutions, to a value ξ/a in semi-dilute solutions where $\xi \sim c_p^{-\gamma}$ is the blob size. For excluded-volume chains the de Gennes exponent γ equals 0.77. Fler and Tuinier^{22,23} have shown that the concentration-dependent cross-over between these two limits is accurately captured by the expression,

$$q_s = 0.865q_R^{0.88}(1 + 3.95y^{2\gamma})^{-0.44} \quad (2)$$

Here y is the reduced polymer concentration, $y = c_p/c_p^*$. In the present paper we focus on the non-equilibrium behaviour of colloid–polymer mixtures prepared with a fixed colloid concentration, $\phi = 0.2$, and polymer concentrations c_p/c_p^* of between 1.98 and 3.97, as detailed in Table 1.

2.4. Confocal microscopy

We use confocal scanning laser microscopy (CSLM) to study the temporal evolution of the bicontinuous network formed in our samples. Because the colloid–polymer mixtures are not buoyancy

Table 1 Colloid–polymer mixtures studied. The polymer concentration in the reservoir is indicated by c_p , $y = c_p/c_p^*$ is the reduced polymer concentration, and $-U_0/k_B T$ is the depletion potential at contact in units of $k_B T$, estimated from eqn (3)

$c_p/\text{g dm}^{-3}$	c_p/c_p^*	$-U_0/k_B T$
0.50	1.98	5.1
0.55	2.18	5.5
0.60	2.38	6.0
0.70	2.78	6.8
0.80	3.17	7.7
1.00	3.97	9.4

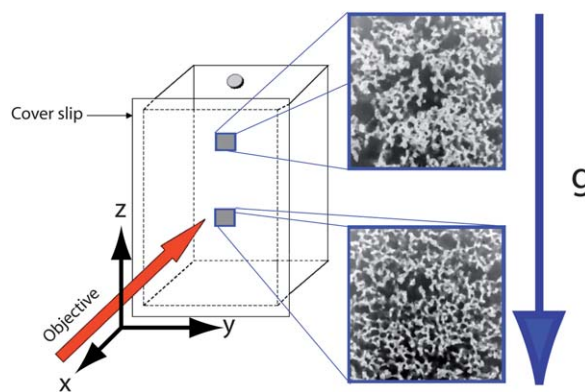


Fig. 2 Schematic of the cell used in the confocal experiments. The morphology of the network is studied in the yz -plane where the z -axis is aligned vertically with gravity and the origin is fixed at the base of the cell. The inset shows images collected at $z = 2$ mm and $z = 4$ mm in a colloid–polymer mixture with $c_p/c_p^* = 2.38$.

matched we expect gravity-driven flow to occur at long observation times so it is important to image the samples in a plane which contains the direction of gravity. A supporting frame was constructed to allow a light microscope (Zeiss, Axioskop S100) to be mounted horizontally, on its side, at right angles to gravity. Two-dimensional fluorescent images were collected in the yz -plane (Fig. 2) by raster scanning the focal point of a $\lambda = 543$ nm laser over an area of $146 \times 146 \mu\text{m}^2$ within the dispersion using a confocal scanning head (Zeiss, LSM Pascal). Images with a size of 1024×1024 pixels were collected in ~ 3 s. We use a high numerical aperture oil immersion objective (1.4NA, 63 x) to image only a thin representative slice parallel to the x -axis. The lateral resolution limit is ~ 400 nm so we do not resolve individual emulsion drops. The microscope detects the fluorescence from excited rhodamine-B dye molecules which are soluble in the continuous phase but insoluble in the PDMS drops so the solvent appears bright and the particles dark. However, for clarity, we have inverted all the micrographs reproduced here so that the colloid-rich phase appears bright and the colloid-poor phase dark. The colloid–polymer samples were studied in large rectangular glass cuvettes with the front wall of the cell constructed from a $170 \mu\text{m}$ thick optical quality cover glass (Fig. 2). The sealed cuvette had a square cross-section with an internal dimension of 13 mm, a height of 30 mm, and contained a small hole at the top of the cell through which the cell was filled. The cell was mounted onto a low profile manual translation stage so that the colloidal dispersion could be imaged at different z -positions, throughout the full height of the sample.

2.5. Rheology

We performed steady-shear rate, oscillatory shear and stress relaxation measurements at $T = 22 \pm 2$ °C using a stress-controlled rheometer (Malvern, Bohlin Gemini HR) as described previously.²⁴ Measurements were made using a double gap geometry with a thin film of silicone oil applied to the surface to minimise evaporation. No pre-shear was applied since this has been shown to densify the network structure.²⁵ Parallel measurements using a vane geometry confirmed the absence of wall slip in these systems.

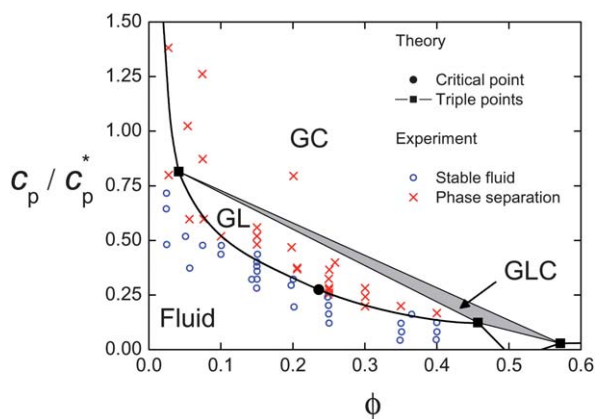


Fig. 3 Phase diagram of the colloid–polymer mixture with $q_R = r_g/a \approx 0.62$. Experimental observation are indicated by open symbols and crosses. The solid curves correspond to the fluid–crystal, gas–liquid, and gas–crystal binodals calculated from GFVT²³ for $q_R = 0.62$. The theoretical prediction for the critical point is shown by the filled circle while the filled squares indicate the compositions of the coexisting gas, liquid and crystal phases in the triple point triangle.

3. Results and discussion

3.1. Phase diagram

To confirm that the origin of the bicontinuous network, evident in Fig. 2, lies in an entropy-driven attraction between the emulsion drops we investigated the phase stability of a range of colloid–polymer mixtures. The phase diagram shown in Fig. 3 summarizes our results. A stable one-phase fluid (circles) is found for low polymer concentrations. At higher polymer concentrations a gas–liquid (GL) phase separation (crosses) is seen. Gas–crystal (GC) and a region of three phase (GLC) coexistence were not observed experimentally, probably because the polydispersity of our particles suppressed crystallization. At higher polymer concentrations, outside the region of the equilibrium data points shown in Fig. 3 we observed non-equilibrium gelation which is detailed below in Sec. 3.2.

We compare the observed phase boundaries with the predictions of the recently proposed generalized free volume theory (GFVT) for the phase behaviour of hard-sphere colloids and non-adsorbing excluded-volume polymer chains.^{22,23} GFVT improves the accuracy at large q_R of the free-volume theory of Lekkerkerker *et al.*²¹ by taking into account the compression of the depletion zone around each particle in a semi-dilute solution and by incorporating non-ideal contributions to the polymer osmotic pressure. Comparison with experimental and simulation data²⁶ have revealed GFVT provides a near quantitative description of the colloid–polymer phase diagram for $q_R \approx 1$. The GFVT predictions for the phase boundaries at the experimentally-measured size ratio $q_R = 0.62$ in a good solvent are shown by the solid lines in Fig. 3. The agreement between the calculated GL binodal and experiments is good, with the vast majority of the experimental two-phase samples lying above the GFVT binodal, confirming that the experimental system may be accurately approximated by a simple mixture of hard spheres and non-adsorbing polymer chains.

Fleer and Tuinier²³ have calculated that the effective colloid pair potential has the strength U_0 , at contact, of

$$-U_0/k_B T = q_s^2 \left(q_s + \frac{3}{2} \right) q_R^{-3} y (1 + 3.77y^{1.31}) \quad (3)$$

and a range q_s given by eqn (2). Since GFVT incorporates the correct dependence of the depletion thickness and osmotic pressure on polymer concentration, eqn (3) should remain valid for any polymer concentration up to and including the semi-dilute regime. For the colloid–polymer mixtures studied here the predicted attraction are relatively weak, with interparticle interaction strength U_0 estimated to vary from between $-5k_B T$ and $-9k_B T$. Increasing c_p leads to a near linear increase in the magnitude of the depletion potential U_0 at contact.

3.2. Confocal microscopy of gelation

Gelation occurs as the system is quenched deep into the two-phase region. Fixing the colloid concentration at $\phi = 0.2$ we mix samples at various polymer concentrations c_p/c_p^* , along a vertical slice through the phase plane which passes reasonably close to the critical point. Mixtures with low c_p , just above the experimental binodal boundary ($c_p/c_p^* = 0.33$), separate into two homogeneous fluid phases, separated by a sharp interface, within about ten minutes. By contrast, in samples with higher polymer concentrations particles aggregate into a long-lived disordered network with colloid-rich and colloid-poor domains which develop, at least visually, a finite low-frequency elastic shear modulus characteristic of a solid-like gel. Oscillatory shear experiments confirm these observations. Fig. 4 shows a representative result of the oscillatory measurements on a sample at $c_p/c_p^* = 3.17$. The storage modulus $G'(\omega)$ exceeds the storage modulus $G''(\omega)$ at all frequencies ω , as expected for a solid. However substantial dissipative loss is evident which suggests that there are significant relaxation processes occurring within the gel. These mechanical characteristics contrast to the situation reported for the arrested gels formed by particles with short-range attractions where $G'(\omega)$ typically exceeds $G''(\omega)$ at high frequencies, by an order of magnitude or more.⁷

To study the structure of the solid network formed we used fluorescence confocal microscopy. Fig. 5 presents examples of

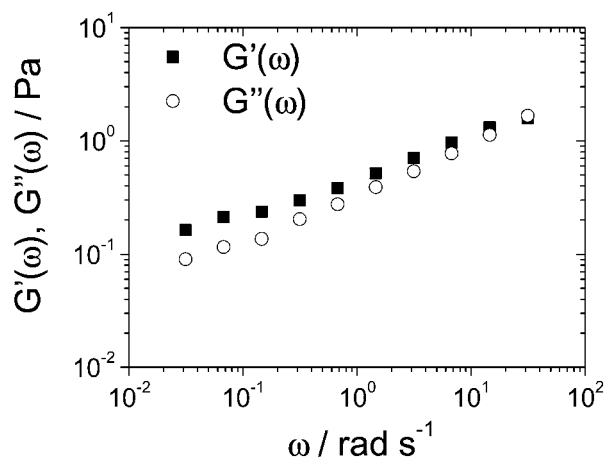


Fig. 4 Elastic modulus $G'(\omega)$ (full symbols) and loss modulus $G''(\omega)$ (open symbols) for a gel formed at a colloid volume fraction of $\phi = 0.20$ and polymer concentration $c_p/c_p^* = 3.17$.

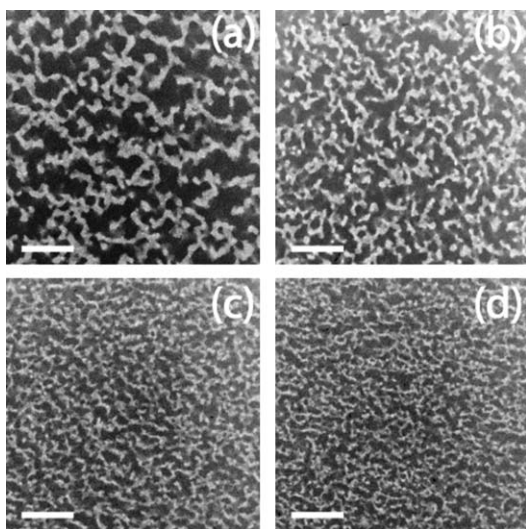


Fig. 5 Confocal micrographs, in the yz -plane, obtained 3600 s after homogenization at polymer concentrations of (a) $c_p/c_p^* = 1.98$, (b) $c_p/c_p^* = 2.38$, (c) $c_p/c_p^* = 3.17$, and (d) $c_p/c_p^* = 3.97$. The particles appear bright in these images and the scale bar corresponds to $30 \mu\text{m}$. Gravity points downwards in all images. All images were collected about 2 mm above the base of a 5 mm tall sample with an initial colloid volume fraction of $\phi = 0.2$.

micrographs of the long range structures obtained at different polymer concentrations c_p/c_p^* . All data were collected from mixtures at a fixed sample age of $t = 3600$ s. In each case we see the formation of a coarse space-spanning network of interconnected colloidal strands. However a close comparison of Fig. 5 (a)–(d) reveals significant changes with c_p/c_p^* . Both the thickness of the particle strands and the relative coarseness of the network reduces sharply as the polymer concentration is increased and the sample is more deeply quenched into the two-phase region of the phase diagram. Essentially an open network of coarse links transforms into a more compact structure of finer chains as c_p/c_p^* is increased. The structures are reminiscent of the patterns generated by classical spinodal decomposition in binary fluids.²⁷ Indeed Fig. 5 (a), in particular, resembles the images of spinodal decomposition observed by Aarts *et al.* in a similar-sized colloid–polymer system ($q_R = 0.56$) just above the critical point.²⁸

3.3. Lack of structural arrest

To explore the similarity between spinodal decomposition and gelation in greater detail we determined the temporal evolution of the network structure by recording a series of 2D confocal images, at a fixed height within the gel, as a function of the sample age t . For each image of width L we calculated the radially-averaged static structure factor $S(q, t)$

$$S(q, t) = \frac{1}{2\pi q \Delta q} \int_{q \in |q'| \leq q + \Delta q} d\mathbf{q}' \langle \tilde{I}(\mathbf{q}', t) \tilde{I}(-\mathbf{q}', t) \rangle \quad (4)$$

where $\tilde{I}(\mathbf{q}, t)$ is the 2D Fourier-transform of the image intensity $I(\mathbf{r}, t)$ recorded from a sample of age t and $\Delta q = 2\pi/L$.

A distinctive hallmark of any diffusion-limited process is the appearance of a peak in $S(q)$ at a finite wavevector q_{max} , which

narrows and moves to smaller q with increasing time t as diffusion has the time to change the structure on larger and larger length scales. Fig. 9 (a) shows examples of the radially-averaged $S(q, t)$ measured at different times t after mixing in a gel formed at a polymer concentration of $c_p/c_p^* = 2.38$. The 2D Fourier-transform displays a ring of high intensity which corresponds to the presence of a large characteristic length scale. The calculated $S(q, t)$ is rather noisy, because of a lack of statistics, so we characterized the average wavenumber by calculating the first moment $\langle q(t) \rangle$ of the scattered intensity,

$$\langle q(t) \rangle = \frac{1}{I_t} \int_{q_1}^{q_2} dq' q S(q', t) \quad (5)$$

where $I_t = \int_{q_1}^{q_2} dq' S(q', t)$ and the integration was performed over the finite interval $q_1 \leq q \leq q_2$, with $q_1 = 0.02 \mu\text{m}^{-1}$ and $q_2 = 0.4 \mu\text{m}^{-1}$. The wavenumber $q(t)$ was converted into a characteristic domain radius using the expression, $R_c(t) = \pi/\langle q(t) \rangle$.

The evolution in time of the characteristic length scale $R_c(t)$ of the gels was extracted from successive confocal images, collected in the yz -plane at a height of $z \approx 2$ mm from suspensions 5 mm high. Identical experiments were carried out with fresh samples at a range of polymer concentrations between 0.5 g dm^{-3} and 1.0 g dm^{-3} . The colloid–polymer mixtures were prepared and constantly stirred using a magnetic stirrer for about 1 h prior to being transferred to the confocal cells and imaged. Confocal images were acquired for ~ 100 h from $t = 10$ s after the cessation of mixing until the point at which gel collapse was seen. The sampling rate was adjusted between 1 image/5 s and 1 image/h to match the age of the gel.

We focus initially on the short-time ($t > 10$ s) behaviour of the characteristic length scale $R_c(t)$ plotted in Fig. 6 (a), where the logarithm of the domain radius $R_c(t)/a$ is shown as a function of the logarithm of time. A striking feature of this data is the lack of domain growth seen at short times ($t \lesssim 25$ s). There are two plausible competing explanations for this behaviour: either the existence of a linear Cahn-regime, similar to that found in the early stages of spinodal decomposition²⁹ or else the existence of a period of kinetic arrest. To distinguish between these two possibilities we first estimate the characteristic times required for (a) the initial formation of a network (percolation) and (b) its subsequent kinetic arrest, using as our guide computer simulation studies^{30–32} of short-range systems. The most convenient unit in which to express these timescales is the Brownian relaxation time τ_B , which we define as the time for a particle to diffuse its own radius by Brownian motion,

$$\tau_B = \frac{\pi \eta a^3}{k_B T} \quad (6)$$

where η is the viscosity of the polymer solution. We estimate τ_B to be between 0.4 s and 0.8 s in our system.

A suspension quenched deep into the two-phase region forms bonds as particles meet by diffusion. This increases the density locally and simultaneously creates regions of low density (holes) elsewhere in the system forming a percolating disordered solid on a time scale τ_p . Brownian dynamics simulations^{30,31} reveal that, at $\phi = 0.2$, percolation is rapid and τ_p is somewhat less than one Brownian relaxation time τ_B . Once the particles have aggregated together in a space-spanning network, a series of complex and

fast collective rearrangements then cause a coarsening of the network whilst it retains its connectivity. In short-range attractive system, recent work⁷⁻¹⁰ has shown that the process of phase separation abruptly halts when the colloid-rich regions solidify in a glass transition. To estimate the time required for kinetic arrest, we use a recent computer simulation study³² which incorporated many-body hydrodynamic interactions. Furukawa and Tanaka³² in a short-range system found evidence for kinetic arrest but only on times $t > 200\tau_B$. Structural arrest, at least in the short-range systems which have been studied to date,^{10,33} persists for two or more decades in time even though individual attractive 'bonds' between particles are not permanent on this time scale. Inserting estimates for τ_B , therefore suggests, that the initial formation of the network will be too fast (<1 s) to be resolved by our confocal technique and, that if gel formation occurs by a process of arrested phase separation, coarsening and domain growth should occur for $t \lesssim 100$ s, with kinetic arrest only being seen on longer time scales. Fig. 6 (a) indicates that, in the experimental system, the growth dynamics is qualitatively different. There is no region of kinetic arrest for $t > 100$ s and the interval where the dominant wavenumber of the network is unchanged is, on the contrary, found at short times ($t \lesssim 25$ s) rather than the long times

expected if kinetic arrest was occurring. We find little evidence for kinetic arrest although we probably need additional measurements at still shorter times $t < 10$ s to definitively verify this conclusion.

The constant domain size seen in Fig. 6 (a) is however fully consistent with the existence of spinodal-like phase dynamics. In the initial stages of phase separation, linear Cahn theory predicts an exponential growth of the fastest-growing density mode. Fourier-transformation of these concentration fluctuations produces a peak in the scattering pattern $S(q,t)$ at a fixed wave-vector which is predicted to grow exponentially with time. Fig. 6 (b) shows the logarithm of the peak intensity $I_c(t)$ versus time t for a number of experiments at different polymer concentrations. Whilst a linear relationship between the logarithm of intensity and time is doubtful, it is clear that the intensity increases rapidly during the period when the domain size is fixed, consistent with the decomposition kinetics expected in the linear regime. A fixed q -peak and growing peak amplitude has been seen previously in comparable mixtures of casein micelles and xanthan,³⁴ although the observations were limited to rather shallow quenches where gelation was not observed. In this work the linear regime was observed on times between 10 s and 100 s after mixing, which is similar to the data shown in Fig. 6 (b), supporting the interpretation that gelation occurs through a spinodal-like mechanism.

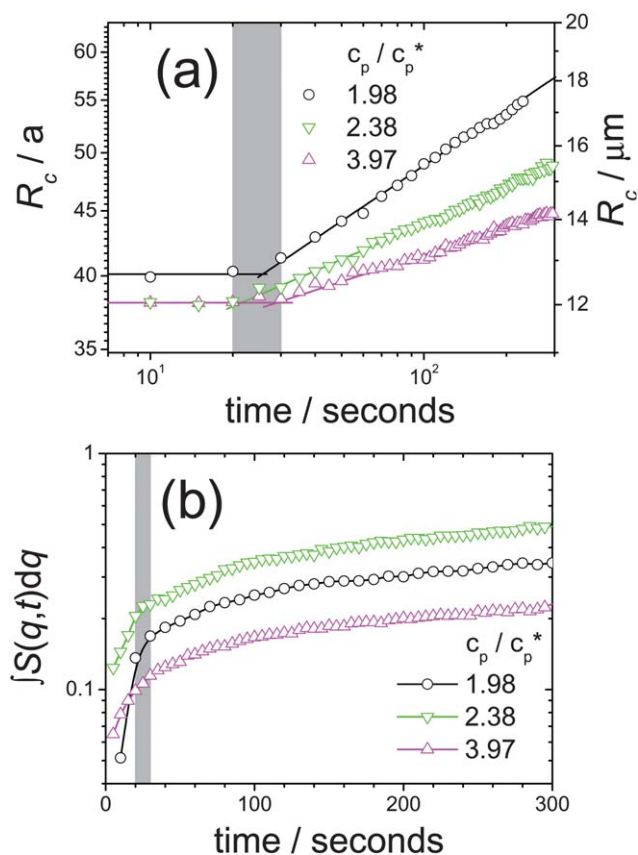


Fig. 6 Domain growth at short times. (a) Plot of the characteristic domain radius $R_c(t)$ vs. t (on a log-log scale) for different polymer concentrations [T_{eff} in brackets]: $c_p/c_p^* = 1.98$ [0.20] (\circ), $c_p/c_p^* = 2.38$ [0.17] (∇), and $c_p/c_p^* = 3.97$ [0.11] (\triangle). The shaded rectangle shows the region where $R_c(t)$ first increases with t . (b) The time evolution of the logarithm of the integrated peak intensity $I_c(t)$. The shaded rectangle shows the same region marked in (a).

3.4. Ageing

Random breaking of particle bonds ensures slow relaxation or ageing occurs within the gel on a time scale set by the 'bond lifetime' τ_{esc} – the time that a particle remains within the range of the mutual attractions of its neighbours. We estimate τ_{esc} by assuming that it equals the mean-first passage Kramers escape time for a Brownian particle confined to a ramp potential with the same range (δ) and depth at contact ($-U_0$) as the predictions of GFVT. The Kramers escape time τ_{esc} in the high-friction, overdamped limit is³⁵

$$\tau_{\text{esc}} = \frac{\delta^2}{D_s} \frac{\exp(-\beta U_0) - (1 - \beta U_0)}{(\beta U_0)^2} \quad (7)$$

where D_s is the short-time self diffusion constant in the network and $\beta = 1/k_B T$. The short-time self diffusion constant in a hard sphere suspension at $\phi = 0.5$, which is a reasonable estimate for ϕ in the densest regions of the gel, is about 20% of the free particle value,³⁶ $D_0 = k_B T / (6\pi\eta a)$, so we take $D_s = 0.2D_0$. The escape time is a rapidly changing function of the polymer concentration c_p since both the well depth at contact $-\beta U_0$ and the range of the attractions, $\delta = a q_s$, depend on c_p in the semi-dilute regime. Using the GFVT predictions (eqn (2) and 3) the bond lifetime lies between ≈ 5 s for the lowest polymer concentrations studied here and ≈ 40 s for the highest. In agreement with these predictions, Fig. 6 (a) reveals the gels begin to coarsen on this timescale. The average domain size increases slowly at first, until for $t > 10^3$ s $R_c(t)$ grows algebraically with time t . The regime of algebraic growth in $R_c(t)$ continues for several decades in t until at long times a region of more rapid growth is seen as the network begins to collapse under gravity. We limit our attention in this section to the ageing characteristics of the gel and postpone a discussion of its collapse until later.

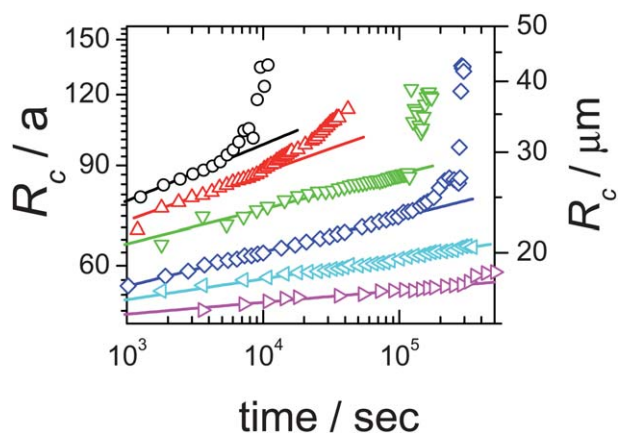


Fig. 7 Domain growth at long times. We plot $R_c(t)$ vs. t (on a log-log scale) for different polymer concentrations [T_{eff} in brackets]: $c_p/c_p^* = 1.98$ [0.20] (\circ), $c_p/c_p^* = 2.18$ [0.18] (\triangle), $c_p/c_p^* = 2.38$ [0.17] (∇), $c_p/c_p^* = 2.78$ [0.15] (\diamond), $c_p/c_p^* = 3.17$ [0.13] (\triangleleft), and $c_p/c_p^* = 3.97$ [0.11] (\triangleright).

Inspection of Fig. 7 shows that the dynamics of ageing is a strong function of the strength of the attractive potential, or equivalently of the effective temperature, $T_{\text{eff}} = k_B T / (-U_0)$. To quantify this dependence we fitted the length scale of the gel to the growth law

$$R_c(t) = R_0 t^\theta \quad (8)$$

with a temperature-dependent effective exponent $\theta(T_{\text{eff}})$ and a temperature-independent prefactor R_0 . The solid lines in Fig. 7 shows that eqn (8) fits the data well. For low T_{eff} , the plots are linear over almost 3 decades in time while for high T_{eff} , the scaling is lost at long times as the gels collapse but eqn (8) still holds at intermediate times.

The phase kinetics in the gel is quantitatively different from the case of spinodal decomposition in isotropic fluids³⁷ where in the viscous hydrodynamic regime the exponent is $\theta = 1$, independent of the quench depth. In the gel, the value of θ is considerably smaller ($\theta < 0.1$) and θ depends sensitively upon the quench temperature T_{eff} . To examine the temperature dependence of θ in greater detail, we plot $1/\theta$ against $1/T_{\text{eff}}$ in Fig. 8. The resulting linear plot suggests the simple functional dependency,

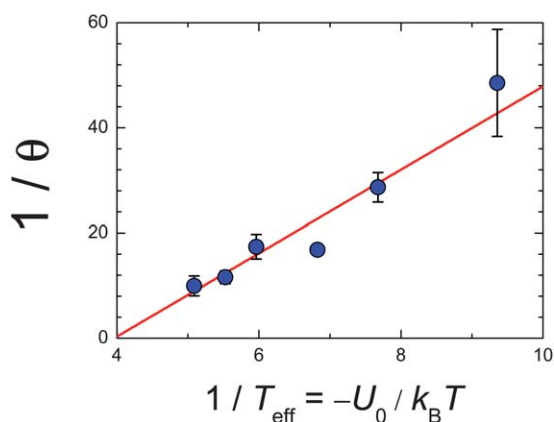


Fig. 8 Variation of the inverse growth exponent $1/\theta$ with the reciprocal temperature $1/T_{\text{eff}}$ for the data shown in Fig. 7.

$$\theta(T_{\text{eff}}) = \left(A + \frac{\varepsilon}{T_{\text{eff}}} \right)^{-1} \quad (9)$$

Linear regression yields $A = -31$ and $\varepsilon = 8$ for the data plotted in Fig. 8. The dependency on T_{eff} suggests that the ageing dynamics is controlled primarily by thermal fluctuations, rather than being stress driven as has been reported previously to be the situation in irreversible gels and jammed systems.^{38,39} Finally, we note that the region to the left of Fig. 8 ($1/T_{\text{eff}} < 4$) is not physically accessible since R_c would need to grow algebraically faster than the case for the phase separation of a binary fluid mixture ($\theta = 1$). Whilst we have not determined exactly the position of the gel boundary in our system, the estimate $k_B T / -U_0 \approx 4$, obtained from Fig. 8, agrees closely with the values determined by Lu *et al.*^{9,10} for the gelation boundary $T_{\text{eff}} \sim 0.2-0.25$, although at a lower q_R .

Any model for the physical mechanism responsible for ageing dynamics must account for the rather simple dependence for θ on the quench depth. A natural starting point for a discussion of ageing is the Ising model following a quench from a high temperature disordered phase to a temperature at which, at equilibrium, the system is ferromagnetically ordered. The far-from-equilibrium evolution is characterized by the growth of domains, with a unique length scale $R_c(t)$ which follows an algebraic growth in time, $R_c(t) \sim t^\theta$. There is a good understanding of the dynamics of phase ordering in uniform pure and isotropic systems.⁴⁰ For the case of a conserved order parameter without hydrodynamic effects (*e.g.* segregation of a binary alloy), we know that $\theta = 1/3$, while when hydrodynamic effects are included (*e.g.* segregation of a binary fluid) we have $\theta = 1$. Such uniform Ising models can not be applicable here since they neglect the consequences of disorder which are an intrinsic feature of a gel. Domain coarsening in a gel requires the cooperative breaking of a relatively large number of inter-particle bonds. However experiments^{41,42} and simulations⁴³⁻⁴⁵ have shown that in dense attractive systems the motion of individual particles is highly heterogeneous that is, there exists a spatial and temporal distributions of mobilities. Frequently it is found that the dynamics has a bimodal character with the coexistence of slow arrested particles and fast diffusing particles. At any time there is a space spanning cluster of particles which behaves as a solid on short time scales coexisting with a sub-population of particles that can more or less freely diffuse through this structure. A simple coarse-grained model which incorporates elements of this physical picture is the random-bond Ising model (RBIM) where the presence of disorder is mimicked by randomizing the exchange interaction between spins.

The Hamiltonian of the RBIM is

$$H = - \sum_{\langle i,j \rangle} J_{ij} \sigma_i \sigma_j \quad (10)$$

where $J_{ij} > 0$ and the subscript i,j denotes a sum over nearest-neighbour pairs only. For a phase separating colloid-polymer mixture the spin σ_i labels whether a lattice site i is occupied by a high density phase (say, $\sigma_i = +1$) or a low density colloid phase ($\sigma_i = -1$). To allow for the different mobilities in the mixture we assume the exchange coupling is drawn from a probability distribution with a width ε which characterizes the amount of

local disorder in the gel. The phase ordering kinetics in the conserved RBIM has been studied extensively in a number of recent papers by Paul, Puri, and Rieger (PPR).^{46,47} The authors show that the presence of disorder considerably slows down the rate of coarsening because of pinning forces associated with the heterogeneity in the random bonds. The domain size is predicted to grow algebraically, in the long-time limit, with an asymptotic temperature-dependent exponent, $\theta = (3 + \varepsilon/T)^{-1}$, which PPR argue arises naturally as a consequence of a repulsive barrier between domains which depends logarithmically on the domain size.⁴⁸ Asymptotic algebraic domain growth and a similar temperature dependence of θ is also seen in Ising spin glass models.⁴⁸ They suggest that the energy barrier scales as $E_B(R_c) \sim \varepsilon \ln(1 + R_c/a)$. Although the exact mechanistic link between the RBIM and our system is unclear the similarity in the functional dependence of $\theta(T)$ seen in both systems suggests that RBIM might provide a useful framework in which to interpret our experimental data. More experiments are required to test the generality of this link.

3.5. Dynamical scaling

If the domain pattern seen at a time t is identical statistically to those recorded at earlier times, apart from a global change of scale, then the structure factor satisfies a dynamical scaling relation.⁴⁰ The phase separation may then be described with one time-dependent parameter, the domain size $R_c(t)$. The inhomogeneities in the particle number density at the point \mathbf{r} with respect to the average number density $\bar{\rho}$, $\delta\rho(\mathbf{r}, t) = \rho(\mathbf{r}, t) - \bar{\rho}$ are then a function of the single length $R_c(t)$, so that the ratio

$$\frac{\langle \delta\rho(\mathbf{r}, t) \delta\rho(\mathbf{r}', t) \rangle}{\langle \delta\rho^2(\mathbf{r}, t) \rangle} = f\left(\frac{|\mathbf{r} - \mathbf{r}'|}{R_c(t)}\right) \quad (11)$$

is time-dependent only as a result of the time dependence of $R_c(t)$. A Fourier transform of eqn (11) reveals that the corresponding static structure factor $S(q, t)$ obeys the scaling law,

$$\frac{S(q, t) \langle q(t)^3 \rangle}{\int_{q_1}^{q_2} dq' q'^2 S(q', t)} = F\left(\frac{q}{\langle q(t) \rangle}\right) \quad (12)$$

where $F(x)$ is a universal scaling function⁴⁹ that depends purely on the wavevector ratio $x = q/\langle q(t) \rangle$ and $\langle q(t) \rangle$ is the average position of the structure factor peak.

Fig. 9 (a) displays experimental scattering curves obtained from the Fourier transform of confocal images, as a function of the age t of the gel. While there is statistical scatter because of the finite size of the images used, the peaks in the structure factors clearly move to smaller q and grow in intensity with t . Fig. 9 (b) shows a test of dynamic scaling in the late stages of ageing ($t > 2$ h). Dynamic scaling holds reasonably well, confirming that the microstructure of the gel may be described by a single age-dependent length $R_c(t)$.

3.6. Stress relaxation

The slow process of continuous coarsening implies that the gels formed could be transient *i.e.* on long timescales the sample might behave as a liquid. To determine if the gels formed here are transient we have extended the mechanical measurements to

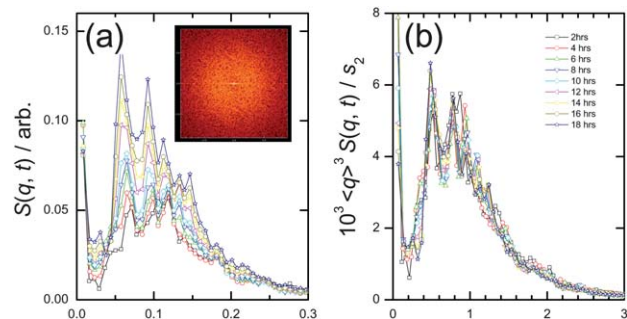


Fig. 9 (a) Radially-averaged scattering peaks obtained from the ageing of a gel formed at a polymer concentration of $c_p/c_p^* = 2.38$. Curves are labeled by the time elapsed after mixing using the symbols detailed in (b). The inset shows an example of the raw two-dimensional Fourier-transform. (b) Dynamic scaling of the data shown in (a) using eqn (12). The normalising factor $s_2 = \int dq' q'^2 S(q', t)$ was calculated in the interval $0.02 \mu\text{m}^{-1} < q < 0.4 \mu\text{m}^{-1}$.

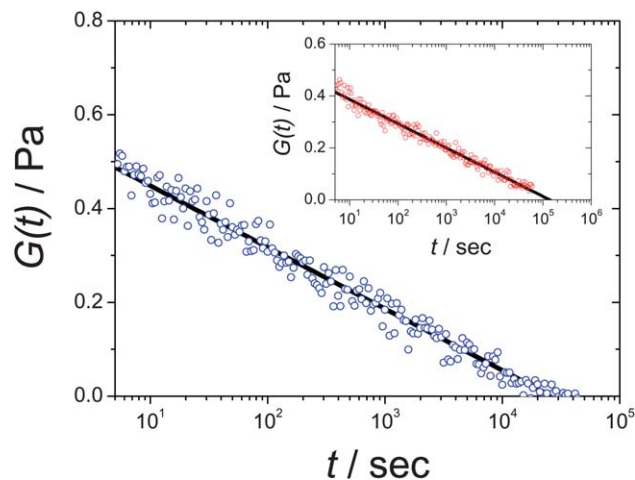


Fig. 10 Stress relaxation modulus $G(t)$ for a gel formed in a sample with $c_p/c_p^* = 3.17$ and $\phi = 0.2$. The data was collected from gels with ages between 10^5 s and 1.5×10^5 s, which showed similar responses, before being averaged. Inset shows result for gel with $c_p/c_p^* = 3.97$. The data was collected from gels with ages between 6×10^4 s and 2.4×10^5 s. A step strain of $\gamma = 0.015$ was applied at $t = 0$.

longer relaxation times using a stress relaxation test. A step strain γ is applied and the time-dependent stress $\sigma(t)$ is recorded for up to 10^5 s to probe the long-time response of the network. Fig. 10 shows the time-dependent decay of the stress relaxation modulus $G(t) = \sigma(t)/\gamma$ measured in gels with $c_p/c_p^* = 3.17$ and $c_p/c_p^* = 3.97$. The modulus $G(t)$ decays at short times ($t < 10^2$ s) as a result of the dissipative processes which contribute to $G''(\omega)$. However Fig. 10 reveals that the gel contains still slower relaxation processes, with $G(t)$ only fully decaying to zero at $t > 3 \times 10^4$ s, confirming the ultimate liquid-like character of the sample. The lifetime τ_r of the transient gel increases with an increase in the quench depth, from $\tau_r \approx 3 \times 10^4$ for $c_p/c_p^* = 3.17$ to $\tau_r \approx 10^5$ for $c_p/c_p^* = 3.97$.

3.7. Gravity-driven gel collapse

Eventually, on times of order of the characteristic relaxation time τ_r , the network of particles loses its elastic nature and collapses

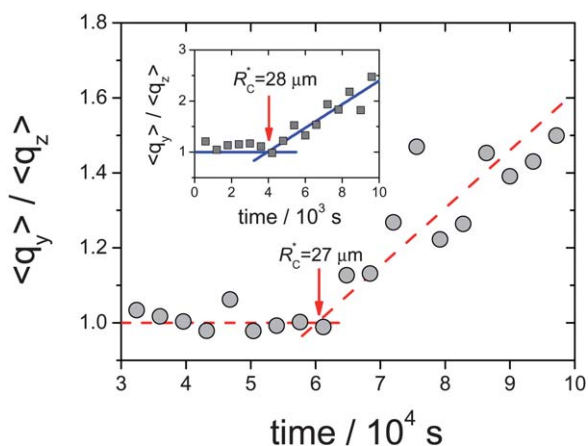


Fig. 11 The ratio $\langle q_y \rangle / \langle q_z \rangle$ of the characteristic wavenumbers of the structure factor in planes perpendicular (y) and parallel to gravity (z) as a function of time. The main figure contains data for a colloidal gel with polymer concentration $c_p/c_p^* = 2.38$ while the inset displays data for a gel with $c_p/c_p^* = 1.98$. The characteristic length scale at the point $t = t^*$ where significant anisotropy first appears is indicated.

under its own weight. The microscopic changes in the morphology of the network which accompanies this gravity-driven collapse are evident in the confocal images of a colloid–polymer mixture ($c_p/c_p^* = 1.98$), reproduced in Fig. 12. We divide the process of phase separation in this sample into three stages. At early times ($t < 10^2$ s), there is an initial formation of a bi-continuous network, which as we have seen occurs on a scale that is too fast to be resolved in our measurements, after which there is a slow growth in the characteristic length $R_c(t)$ (see data in Fig. 7). On intermediate times $10^2 < t < 4 \times 10^3$ s, the network coarsens as the characteristic length scale grows algebraically with age, $R_c \sim t^\theta$, with a fixed temperature-dependent exponent $\theta(T_{\text{eff}})$. At long times $t > 4 \times 10^3$, the characteristic length grows more rapidly and

a plot of $R_c(t)$ versus t deviates increasingly from the algebraic growth regime established at intermediate times. Confocal images show that in this late stage the network becomes increasingly anisotropic (compare for instance, the images at 7200 s and 4200 s in Fig. 12). We demonstrate the development of anisotropy in the gel structure by following the time evolution of the q -position of the scattering peak $S(q,t)$ for wave vectors either parallel or perpendicular to the direction of gravity. The 1D-Fourier-transform of each horizontal row of pixels in the image was performed and averaged together to yield the mean position $\langle q_y \rangle$ of the scattering peak along the y -axis, perpendicular to the direction of gravity. A similar calculation was performed on each vertical column of pixels to estimate $\langle q_z \rangle$, the mean position of the scattering peak parallel to gravity. In fig. 11, we plot the wave number ratio $\langle q_y \rangle / \langle q_z \rangle$ versus the age of the gel, for a number of different gels. In each case, there is a comparable behaviour. At early times, the gel is essentially isotropic with $\langle q_y \rangle / \langle q_z \rangle \approx 1$. However with increasing age a clear break appears at $t = t^*$, after which the wave vector ratio abruptly increases and the microstructure of the gel becomes anisotropic. Interestingly, we note that the effect of gravity on the gel is to stretch the domains along the gravitational z -direction compared to the orthogonal y -axis. The extension recorded is presumably a consequence of the effect of adhesion to the cell walls which prevents the macroscopic shrinking of the gel. Identifying the point where $\langle q_y \rangle / \langle q_z \rangle$ abruptly increases as the time t^* at which gravitational collapse is initiated we note that the characteristic length scale at collapse is $27 \mu\text{m}$. Repeating the measurements of anisotropy in other colloid–polymer mixtures (see Fig. 11) reveals a very similar sequence of behaviour and an essentially constant length scale at collapse of $\approx 27 \mu\text{m}$.

To account for the existence of a critical length scale at collapse, we consider the gravitational stability of a flat interface formed between colloid-rich and colloid-poor phases. On time scales $t > \tau_r$, we can ignore elastic effects and treat the gel as a system of random bicontinuous interfaces which separate two

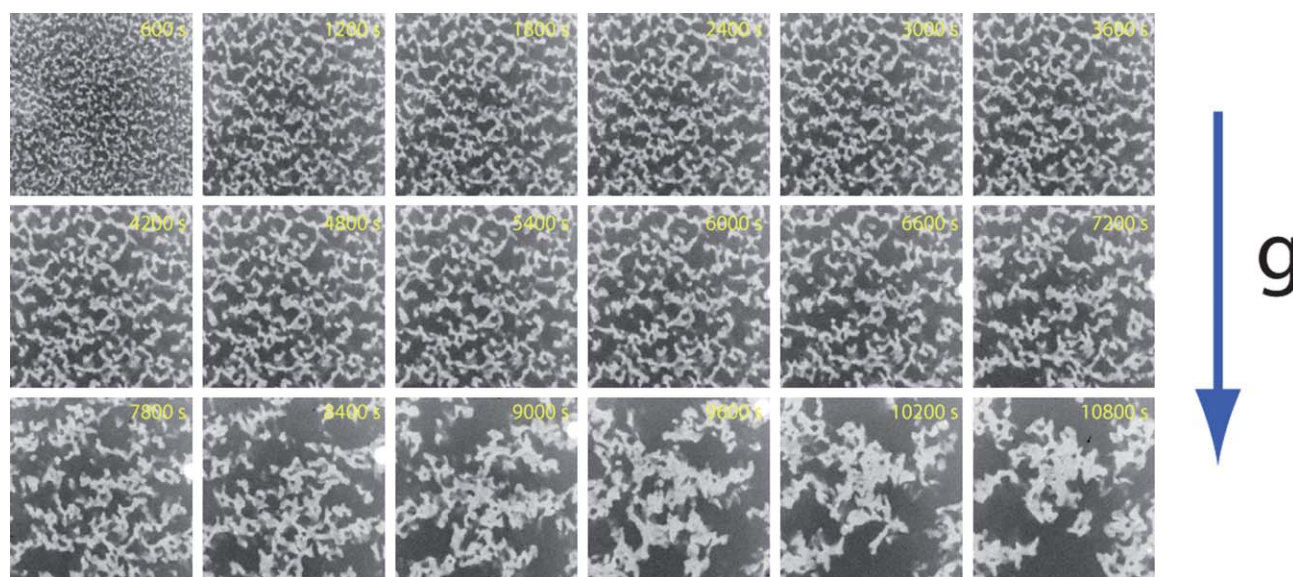


Fig. 12 Confocal images ($146 \times 146 \mu\text{m}^2$) of coarsening and collapse of a gel formed in a colloid–polymer mixture with $\phi = 0.2$ and $c_p/c_p^* = 1.98$. In all images the particles are bright and gravity points downwards. The dispersion had a height of 5.1 mm and the images were recorded at a height of ~ 2 mm above the base of the cell.

fluids with different mass densities $\delta\rho$. A horizontal interface with a lighter fluid phase below a heavy fluid phase is clearly gravitationally unstable; a long wavelength fluctuation of the surface away from its initial flat geometry leads to a pressure imbalance which amplifies the fluctuation. In contrast, small wavelength fluctuations of the interface are suppressed by the increased area of the interface generated, which costs interfacial energy. The competition between interfacial energy and gravity generates a critical length scale L_c for the ensuing Rayleigh–Taylor instability.²⁸ An interface of length $L < L_c$ remains stable, while for $L > L_c$ an unstable mode appears whose amplitude grows in time. The critical threshold value is $L_c = 2\pi\lambda_{\text{cap}}$ ⁵⁰ where λ_{cap} is the capillary length

$$\lambda_{\text{cap}} = \sqrt{\frac{\gamma}{g\delta\rho}} \quad (13)$$

and γ is the interfacial tension between the two fluids. To estimate γ we use the approximate expression,⁵¹ $\gamma = U_0\phi/(2a)^2$. Taking U_0 as $5.1k_B T$ we estimate $\gamma \approx 1.1 \times 10^{-8} \text{ N m}^{-1}$. Since the quench is deep we assume the gas phase is very dilute in colloid $\phi \approx 0$ and the volume fraction of the dense phase is $\phi \approx 0.5$. Hence $\delta\rho = 65 \text{ kg m}^{-3}$. Using these values the length of the unstable mode is $L_c \approx 26 \mu\text{m}$, which is in good agreement with the critical length scale observed experimentally.

4. Summary and conclusions

Using a combination of real space imaging and rheology we have studied mixtures of colloid and non-adsorbing polymer with a large size ratio, $q_R = 0.62$, so that the particle interact through weak long-ranged attractions. We demonstrate concentrated dispersions of these particles form a long-lived viscoelastic gel which ultimately decays and collapses under its own weight. Confocal microscopy reveals the formation, at high polymer concentrations, of a bi-continuous network of colloid-rich and colloid-poor domains. Stress relaxation measurements confirm that, while at short times the gel shows appreciable elasticity, on long time scales ($t > 10^4 \text{ s}$) the gel has a liquid-like character with a zero long-time elastic modulus. By Fourier transforming two-dimensional images of the gel we determine an averaged structure factor $S(q,t)$ which in all cases displays a peak at small wave numbers. From the position of the ring we extract the characteristic radius $R_c(t)$ of the network, as a function of its age. We find three distinct regimes in the time evolution of $R_c(t)$, reminiscent of the linear, late and gravity-dominated regimes of coarsening seen in classical spinodal decomposition (SD) kinetics of binary fluids.³⁷ At the shortest times experimentally accessible to us ($t > 10 \text{ s}$), we find evidence for a linear Cahn-regime where the position of the peak in the structure factor is unchanged with t but whose intensity grows rapidly with t . After about $t \sim 30 \text{ s}$ the peak starts to collapse to small wavenumbers as it continues to grow in intensity. At long times ($t > 10^3 \text{ s}$), the characteristic scale of the gel follows an algebraic form $R_c(t) \sim t^\theta$ with a growth exponent θ which reduces with increasing interparticle attractions. Defining an effective quench temperature of $T_{\text{eff}} = k_B T / (-U_0)$ we find that the temperature dependence of θ follows the simple relation, $\theta(T_{\text{eff}}) = \left(A + \frac{\epsilon}{T_{\text{eff}}}\right)^{-1}$. At long times, the

structure factor $S(q,t)$ at any time t collapses onto a single master curve when scaled according to the expression, $S(q,t)\langle q(t) \rangle^3 / s_2$ where the normalizing factor $s_2 = \int dq' q'^2 S(q',t)$. Finally when the characteristic length reaches a critical size of order $2\pi\lambda_{\text{cap}}$ the network structure becomes anisotropic and the transient network begins to collapse due to gravity.

In conclusion, these results highlight the significance of the range of the attractive potential for the mechanism of gelation. Whilst for particles with short-ranged attractions gelation is generally believed to proceed *via* an arrested SD, this seems not to be the case in systems with long-range attractions. On the contrary, in such long-range systems we find phase separation kinetics which although reminiscent of classical SD display *no* features, as far as we can tell, of kinetic arrest. The process of gelation seems to be qualitatively different in systems with long-range attractions. Quenching into the two-phase region for large q_R generates a long-lived viscoelastic gel which ultimately decays and collapses under its own weight. The phase separation kinetics in these materials is clearly not the usual SD seen in binary fluids. The value of the growth exponent θ is smaller than the conventional late stage value found in fluid-fluid phase separations ($\theta = 1$) and the exponent decreases with increasing quench depth. The microscopic explanation of these phase dynamics is not clear but some of the details are qualitatively reproduced by an Ising model with quenched disorder. Given the keen interest in tailoring the structure and dynamics of gels for diverse applications in consumer products, materials and food science these findings suggest new avenues for the formulation of complex fluids.

Acknowledgements

We thank an anonymous referee for a number of very helpful suggestions. We would also like to thank Richard Buscall, Peter Lu, Peter Pusey, Paddy Royall, and Isla Zhang for illuminating discussions and Humphrey Yeung for his assistance with rheology measurements. This work was supported jointly by Bayer CropScience and the UK Engineering and Physical Sciences Research Council through the award of an Industrial CASE award to LJT from the Chemistry Innovation KTN.

Notes and references

- 1 E. Zaccarelli, *J. Phys.: Condens. Matter*, 2007, **19**, 323101.
- 2 R. Mezzenga, P. Schurtenberger, A. Burbidge and M. Michel, *Nat. Mater.*, 2005, **4**, 729–740.
- 3 R. Piazza, *Curr. Opin. Colloid Interface Sci.*, 2004, **8**, 515–522.
- 4 J. I. Clark and D. Carper, *Proc. Natl. Acad. Sci. U. S. A.*, 1987, **84**, 122–125.
- 5 M. Manno, P. L. San Biagio and M. U. Palma, *Proteins: Structure, Function, and Bioinformatics*, 2004, **55**, 169–176.
- 6 J. C. Conrad, H. M. Wyss, V. Trappe, S. Manley, K. Miyazaki, L. J. Kaufman, A. B. Schofield, D. R. Reichman and D. A. Weitz, *J. Rheol.*, 2010, **54**, 421–438.
- 7 F. Cardinaux, T. Gibaud, A. Stradner and P. Schurtenberger, *Phys. Rev. Lett.*, 2007, **99**, 118301.
- 8 T. Gibaud and P. Schurtenberger, *J. Phys.: Condens. Matter*, 2009, **21**, 322201.
- 9 P. J. Lu, E. Zaccarelli, F. Ciulla, A. B. Schofield, F. Sciortino and D. A. Weitz, *Nature*, 2008, **453**, 499–503.
- 10 E. Zaccarelli, P. J. Lu, F. Ciulla, D. A. Weitz and F. Sciortino, *J. Phys.: Condens. Matter*, 2008, **20**, 494242.
- 11 G. Foffi, C. D. Michele, F. Sciortino and P. Tartaglia, *Phys. Rev. Lett.*, 2005, **94**, 078301.

- 12 G. Foffi, G. D. McCullagh, A. Lawlor, E. Zaccarelli, K. A. Dawson, F. Sciortino, P. Tartaglia, D. Pini and G. Stell, *Phys. Rev. E: Stat. Phys., Plasmas, Fluids, Relat. Interdiscip. Top.*, 2002, **65**, 031407.
- 13 T. Coviello, K. Kajiwara, W. Burchard, M. Dentini and V. Crescenzi, *Macromolecules*, 1986, **19**, 2826–2831.
- 14 T. Sato, S. Kojima, T. Norisuye and H. Fujita, *Polym. J.*, 1984, **16**, 423–429.
- 15 T. Sho, T. Sato and T. Norisuye, *Biophys. Chem.*, 1986, **25**, 307–313.
- 16 F. Franks and D. J. G. Ives, *Q. Rev. Chem. Soc.*, 1966, **20**, 1–44.
- 17 M. Bohdanecky, *Macromolecules*, 1983, **16**, 1483–1492.
- 18 H. Yamakawa and M. Fujii, *Macromolecules*, 1974, **7**, 128–135.
- 19 H. Benoit and P. Doty, *J. Phys. Chem.*, 1954, **57**, 958–963.
- 20 M. Schmidt, *Macromolecules*, 1984, **17**, 553–560.
- 21 H. N. W. Lekkerkerker, W. C. K. Poon, P. N. Pusey, A. Stroobants and P. B. Warren, *Europhys. Lett.*, 1992, **20**, 559–564.
- 22 G. J. Fleer and R. Tuinier, *Phys. Rev. E: Stat., Nonlinear, Soft Matter Phys.*, 2007, **76**, 041802.
- 23 G. J. Fleer and R. Tuinier, *Adv. Colloid Interface Sci.*, 2008, **143**, 1–47.
- 24 M. A. Faers, *Adv. Colloid Interface Sci.*, 2003, **106**, 23–54.
- 25 C. J. Rueb and C. F. Zukoski, *J. Rheol.*, 1997, **41**, 197–218.
- 26 R. Tuinier, P. A. Smith, W. C. K. Poon, S. U. Egelhaaf, D. Aarts, H. N. W. Lekkerkerker and G. J. Fleer, *Europhys. Lett.*, 2008, **82**, 68002.
- 27 P. Guenoun, R. Gastaud, F. Perrot and D. Beysens, *Phys. Rev. A*, 1987, **36**, 4876–4890.
- 28 D. Aarts, R. P. A. Dullens and H. N. W. Lekkerkerker, *New J. Phys.*, 2005, **7**, 40.
- 29 J. W. Cahn, *J. Chem. Phys.*, 1965, **42**, 93–99.
- 30 R. J. M. d'Arjuzon, W. Frith and J. R. Melrose, *Phys. Rev. E: Stat. Phys., Plasmas, Fluids, Relat. Interdiscip. Top.*, 2003, **67**, 061404.
- 31 K. G. Soga, J. R. Melrose and R. C. Ball, *J. Chem. Phys.*, 1998, **108**, 6026–6032.
- 32 A. Furukawa and H. Tanaka, *Phys. Rev. Lett.*, 2010, **104**, 245702.
- 33 G. Foffi, C. De Michele, F. Sciortino and P. Tartaglia, *J. Chem. Phys.*, 2005, **122**, 224903.
- 34 S. Bhat, R. Tuinier and P. Schurtenberger, *J. Phys.: Condens. Matter*, 2006, **18**, L339–L346.
- 35 P. A. Smith, G. Petekidis, S. U. Egelhaaf and W. C. K. Poon, *Phys. Rev. E: Stat., Nonlinear, Soft Matter Phys.*, 2007, **76**, 041402.
- 36 P. N. Pusey, *Liquids, Freezing and Glass transition*, North Holland, Amsterdam, 1991, pp. 763–942.
- 37 E. D. Siggia, *Phys. Rev. A*, 1979, **20**, 595–605.
- 38 L. Cipelletti, S. Manley, R. C. Ball and D. A. Weitz, *Phys. Rev. Lett.*, 2000, **84**, 2275–2278.
- 39 L. Cipelletti, L. Ramos, S. Manley, E. Pitard, D. A. Weitz, E. E. Pashkovski and M. Johansson, *Faraday Discuss.*, 2003, **123**, 237–251.
- 40 A. J. Bray, *Adv. Phys.*, 1994, **43**, 357–459.
- 41 P. Mayer, H. Bissig, L. Berthier, L. Cipelletti, J. P. Garrahan, P. Sollich and V. Trappe, *Phys. Rev. Lett.*, 2004, **93**, 115701.
- 42 J. D. Clare, K. Michael and J. S. Michael, *Phys. Rev. E: Stat., Nonlinear, Soft Matter Phys.*, 2008, **77**, 050401.
- 43 P. Chaudhuri, L. Berthier, P. I. Hurtado and W. Kob, *Phys. Rev. E: Stat., Nonlinear, Soft Matter Phys.*, 2010, **81**, 040502(R).
- 44 A. M. Puertas, M. Fuchs and M. E. Cates, *J. Chem. Phys.*, 2004, **121**, 2813–2822.
- 45 A. M. Puertas, M. Fuchs and M. E. Cates, *Phys. Rev. E: Stat., Nonlinear, Soft Matter Phys.*, 2007, **75**, 031401.
- 46 R. Paul, S. Puri and H. Rieger, *Phys. Rev. E: Stat., Nonlinear, Soft Matter Phys.*, 2005, **71**, 061109.
- 47 R. Paul, S. Puri and H. Rieger, *Europhys. Lett.*, 2004, **68**, 881.
- 48 Asymptotic algebraic domain growth and a similar temperature dependence of θ is also seen in Ising spin glass models⁵².
- 49 J. K. G. Dhont, *J. Chem. Phys.*, 1996, **105**, 5112–5125.
- 50 E. Guyon, J. P. Hulin, L. Petit and C. Matescu, *Physical Hydrodynamics*, Oxford University Press, Oxford, 2001.
- 51 A. E. Bailey, W. C. K. Poon, R. J. Christianson, A. B. Schofield, U. Gasser, V. Prasad, S. Manley, P. N. Segre, L. Cipelletti, W. V. Meyer, M. P. Doherty, S. Sankaran, A. L. Jankovsky, W. L. Shiley, J. P. Bowen, J. C. Eggers, C. Kurta, J. T. Lorik, P. N. Pusey and D. A. Weitz, *Phys. Rev. Lett.*, 2007, **99**, 205701.
- 52 H. G. Katzgraber and I. A. Campbell, *Phys. Rev. B: Condens. Matter Mater. Phys.*, 2005, **72**, 014462.